https://doi.org/10.5194/acp-2021-875
Preprint. Discussion started: 1 November 2021

Atmospheric Chemistry and Physics Discussions

Enhanced photodegradation of dimethoxybenzene isomers in/on ice compared to in aqueous solution

Ted Hullar[1], Theo Tran[1], Zekun Chen[2], Fernanda Bononi[2], Oliver Palmer[1,3], Davide Donadio[2], and Cort Anastasio[1,*]

[1] Department of Land, Air and Water Resources, University of California, Davis, One Shields Avenue, Davis, CA 95616, USA

[2] Department of Chemistry, University of California, Davis, One Shields Avenue, Davis, CA 95616, USA

[3] Now at TeraPore Technologies, 407 Cabot Road, South San Francisco, CA 94080

[*] Corresponding author, canastasio@ucdavis.edu, (530) 754-6095

Abstract

Photochemical reactions of contaminants in snow and ice can be important sources and sinks for various organic and inorganic compounds. Snow contaminants can be found in the bulk ice matrix, in internal liquid-like regions (LLRs), or in quasi-liquid layers (QLLs) at the air-ice interface, where they can readily exchange with the firn air. Some studies have reported that direct photochemical reactions occur faster in LLRs and QLLs than in aqueous solution, while others have found similar rates. Here, we measure the photodegradation rate constants of the three dimethoxybenzene isomers under varying experimental conditions, including in aqueous solution, in LLRs, and at the air-ice interface of nature-identical snow. Relative to aqueous solution, we find modest photodegradation enhancements (3- and 6-fold) in LLRs for two of the isomers, and larger enhancements (15- to 30-fold) at the air-ice interface for all three isomers. We use computational modeling to assess the impact of light absorbance changes on photodegradation rate enhancements at the interface. We find small (2-5 nm) bathochromic (red) absorbance shifts at the interface relative to in solution, which increases light absorption, but this factor only accounts for less than 50% of the measured rate constant enhancements. The major factor responsible for photodegradation rate enhancements at the air-ice interface appears to be more efficient photodecay: estimated dimethoxybenzene quantum yields are 6- to 24-fold larger at the interface compared to in aqueous solution and account for the majority (51-96%) of the observed enhancements. Using a hypothetical model compound with an assumed Gaussian-shaped absorbance peak, we find that a shift in the peak to higher or lower wavelengths can have a minor to substantial impact on photodecay rate constants, depending on the original location of the peak and the magnitude of the shift. Changes in other peak properties at the air-ice interface, such as peak width and height (i.e., molar absorptivity) can also impact rates of light absorption and direct photodecay.

https://doi.org/10.5194/acp-2021-875
Preprint. Discussion started: 1 November 2021

Atmospheric Chemistry and Physics Discussions

1. Introduction

Snow and ice contain a wide variety of chemical compounds (Grannas et al. 2006), which can be transformed via photochemical reactions (Bartels-Rausch et al. 2014, Domine and Shepson 2002, Grannas et al. 2007). While snow and ice are comprised primarily of crystalline water ice, under environmental conditions there are also small areas of disordered water molecules that contain most of the solutes present in a snowpack (Barret et al. 2011, Bartels-Rausch et al. 2014, Grannas et al. 2007, Jacobi et al. 2004). At the air-ice interface, these regions are called quasi-liquid layers (QLLs), while those located at ice grain boundaries and other locations within the ice matrix are referred to as liquid-like regions (LLRs). Photochemistry can be important in snowpacks (Grannas et al. 2007), as light can penetrate tens of centimeters below the snow surface (France et al. 2011, Galbavy et al. 2007, Phillips and Simpson 2005). Photochemical reactions are classified as either direct – where a compound absorbs sunlight and is transformed – or indirect – where a reactive species (e.g., hydroxyl radical) formed from a direct photoreaction reacts with the compound of interest.

Despite their importance, only a small number of direct photochemical reactions have been studied in/on ice, with variable and occasionally conflicting findings. Measurements of direct photodegradation rates for a number of inorganic solutes (e.g., nitrate, nitrite, and hydrogen peroxide) found the same temperature dependence in aqueous solution and LLRs, suggesting both compartments provide similar environments for chemical reactions (Chu and Anastasio 2003, Chu and Anastasio 2005, Chu and Anastasio 2007). The picture is more complicated for PAHs (polycyclic aromatic hydrocarbons). Two studies found little difference in PAH photochemistry in/on ice compared to solution: phenanthrene, pyrene, and fluoranthene had similar photodegradation rates in aqueous solution and in LLRs (Ram and Anastasio 2009), while anthracene and pyrene had similar rates in aqueous solution, LLRs, and at the air-ice inteface (QLLs) (Hullar et al. 2018). However, two other studies reported that the photodecay of anthracene and naphthalene were faster in LLRs and at the air-ice interface compared to in solution (2007, Kahan et al. 2010). Harmine has also been reported to photodegrade faster at the air-ice interface (Kahan et al. 2010). Most recently, we found that guaiacol photodegradation was somewhat faster in LLRs, and considerably faster at the-air ice interface, than in aqueous solution (Hullar et al. 2020).

To evaluate the possible causes of photodegradation enhancements in/on ice compared to solution, consider the variables that control the direct photodecay rate for a chemical "C" (M s^{-1}) (Chu and Anastasio 2003):

$$\frac{d[C]}{dt} = -\sum_{\lambda} \frac{2303}{N_A} I_\lambda \Delta\lambda \Phi_{C,\lambda} \varepsilon_{C,\lambda} [C] \qquad (1)$$

where 2303 is a factor for units (1000 cm^3 L^{-1}) and for converting the measurements from base 10 to base *e*, N_A is Avogadro's number (6.022 × 10^{23} molecules mol^{-1}), I_λ is the actinic flux at each wavelength (photons cm^{-2} s^{-1} nm^{-1}), $\Delta\lambda$ is the wavelength interval between photon flux data points (nm), $\varepsilon_{C,\lambda}$ is the molar absorptivity for C (M^{-1} cm^{-1}), $\Phi_{C,\lambda}$ is the quantum yield for loss of C (molecule $photon^{-1}$), and [C] is the concentration (M). Based on equation 1, three factors could increase reaction rates in/on ice relative to solution: higher local photon fluxes, a bathochromic

https://doi.org/10.5194/acp-2021-875
Preprint. Discussion started: 1 November 2021


Atmospheric Chemistry and Physics Discussions

(red) shift in molar absorptivity ($\varepsilon_{C,\lambda}$) towards longer wavelengths, which have greater photon fluxes, or larger quantum yields.

Many previous studies did not measure photon fluxes at the point of the reaction, so it is difficult to accurately determine the significance of local flux differences in accounting for photodecay enhancements in, or on, ice. However, measurements in different solute locations, e.g., in solution, in LLRs, and at the air-ice interface, found that photon fluxes varied by less than a factor of 1.5 (McFall and Anastasio 2016). In addition, in our recent work with guaiacol we normalized photodecay rate constants by photon flux but still saw large differences in rate constants between solution, in ice, and at the air-ice interface (Hullar et al. 2020). Thus local photon flux differences do not appear to a major factor in observed reaction rate enhancements in/on ice.

Because solar photon fluxes increase by several orders of magnitude between 295 and 400 nm (Madronich and Flocke 1998), even a small shift in compound absorbance towards longer wavelengths (i.e., a red, or bathochromic, shift) could substantially increase the amount of light absorbed by a compound, increasing its reaction rate. Several studies have measured absorbance shifts for compounds in LLRs and at the air-ice interface relative to solution (Corrochano et al. 2017, Heger et al. 2005, Kahan and Donaldson 2010, Kania et al. 2014, Krausko et al. 2015, Malongwe et al. 2016, Matykiewiczová et al. 2007). Although the absorbance of some compounds was the same as in aqueous solution, other chemicals shifted by up to 15 nm either to the red or blue (i.e., a hypsochromic shift). Unfortunately, measuring a compound's absorbance at the air-ice interface can be challenging. Accurate absorbance measurements typically require relatively high concentrations, which can lead to aggregation on the ice surface, potentially influencing the absorption characteristics. To avoid this problem, we recently used molecular modeling to estimate the absorbance shift for guaiacol at the air-ice interface (Bononi et al. 2020, Hullar et al. 2020). While we did find a slight bathochromic shift (5 nm), this shift explained less than 10% of the enhanced reaction rates found at the interface.

Finally, an increased quantum yield at the air-ice interface could explain a faster reaction rate, due to a greater fraction of absorbed photons resulting in loss of the chemical. Some studies suggest LLRs and solution represent similar reaction environments (Chu and Anastasio 2003, Chu and Anastasio 2005, Chu and Anastasio 2007, Ram and Anastasio 2009), while others have found higher quantum yields at the air-ice interface (Hullar et al. 2020, 2018, Zhu et al. 2010). Our recent work with guaiacol (Hullar et al. 2020) found that changes in the quantum yield were the dominant contributor to reaction rate differences between aqueous solution, LLRs, and QLLs, with values up to 40-fold higher at the air-ice interface compared to solution.

Taken together, previous studies show the importance of determining various factors to understand the reasons for enhanced chemical reaction rates in snow and ice. In particular, our recent results (Hullar et al. 2020) indicate that the direct photodecay of guaiacol is different in aqueous solution, LLRs, and QLLs, and demonstrated how molecular modeling can be used to assess the relative contributions of changes in light absorbance and quantum yield. Here, we extend those results to three additional organic compounds: 1,2-, 1,3-, and 1,4-dimethoxybenzene (abbreviated 1,2-DMOB, 1,3-DMOB, and 1,4-DMOB, respectively). 1,2- and 1,3-DMOB have been reported to photodegrade slowly, with 1,4-DMOB loss being somewhat faster (Amaine et al. 1993). We measure the direct photochemical reaction rate constants of these compounds in aqueous solution, LLRs, and QLLs, normalizing each to the measured photon flux for a given sample type. To assess the contribution of absorbance shifts,

https://doi.org/10.5194/acp-2021-875
Preprint. Discussion started: 1 November 2021

Atmospheric Chemistry and Physics Discussions

we model DMOB absorbance in aqueous solution and on an ice surface. As with guaiacol, the DMOBs are all doubly-substituted aromatic rings; however, the hydroxyl group of guaiacol is replaced by a methoxy group, eliminating the possible unwanted reaction with triplet excited states ($^3C^*$). Further, the three isomers provide the opportunity to examine how structural differences can influence light absorption, quantum yields, and ultimately photochemical reactivity. To more broadly examine the importance of changes in light absorption on photodecay, we also quantify how changes in the absorbance peak location, maximum absorbance, and absorption peak shape affect photochemical reaction rate constants and lifetimes.

2 Methods

2.1 Materials

1,2-, 1,3-, and 1,4-DMOB (99, >98, and 99% purity, respectively) were from Aldrich. Acetonitrile (HPLC grade) was from Acros. 2-nitrobenzaldehyde (2NB, 98%) was from Sigma-Aldrich. High purity water ("MQ") was from house-produced reverse osmosis water run through a Barnstead International DO813 activated carbon cartridge and a Millipore Milli-Q Advantage A10 system ($\geq$ 18.2 MΩ cm).

2.2 Sample preparation

We placed samples in 10-ml glass beakers (Pyrex) and covered them with nylon film (McMaster-Carr, approximately 25 µm thick, secured in place with an o-ring) to reduce evaporation and contamination while allowing sample illumination. As discussed in our previous work with guaiacol (Hullar et al. 2020), we prepared samples using one of five different methods: 1) in an aqueous solution, where we dissolved the test compound in MQ water to give a final concentration of 1.0 µM, then we placed 10 ml of solution in a beaker and covered. 2) Freezer frozen solution, prepared identically to aqueous solution, then placed in a laboratory freezer (-20 °C) for at least 3 hours. 3) Liquid nitrogen frozen solution, which we prepared identically to aqueous solution, then placed it in a pan filled to a depth of 2 cm with liquid nitrogen; sample freezing took approximately 90 seconds. 4) Vapor deposition of gas-phase test compound to the surface of ice. Following an approach previously described (Hullar et al. 2020, Hullar et al. 2018), we placed 10 ml of MQ water in a beaker, covered it with film, and froze it in a laboratory freezer. We removed and uncovered the frozen samples, and directed a nitrogen stream containing gas-phase dimethoxybenzene at the ice surface for 15 or 30 s. We then recovered the samples and placed them back in a laboratory freezer. 5) Vapor deposited to nature-identical snow, which was produced as described in our previous work (Hullar et al. 2020). To deposit dimethoxybenzene onto the snow, we passed nitrogen from a tank in the cold room first through 500 ml of laboratory-made snow (to condition the nitrogen stream with water vapor), then through a glass container holding 0.4 g of DMOB, and then through a 500- or 1000-ml HDPE bottle holding the snow to be illuminated. 1,2-DMOB is a liquid at room temperature but a solid at -20 °C, while 1,3-DMOB is a liquid at both temperatures and 1,4-DMOB a solid. We then gently mixed the treated snow and transferred it to beakers, tamped it down 10 mm below the top edge of the beaker, and covered it with nylon film.

2.3 Sample illumination, actinometry, and chemical analysis

https://doi.org/10.5194/acp-2021-875
Preprint. Discussion started: 1 November 2021

Atmospheric Chemistry and Physics Discussions

Sample illumination followed the method described previously (Hullar et al. 2020). We set sample beakers upright in a drilled aluminum block set within a temperature-controlled chamber; dark samples were completely covered with aluminum foil and placed in the aluminum block next to the illuminated samples. The samples were held at 5 °C (for aqueous) or -10 °C (for ice and snow). The light source was a 1000 W Xenon arc lamp filtered with an AM1.5 airmass filter (Sciencetech) and a 295-nm longpass filter (Andover Corporation) to approximate polar sunlight and a 400-nm shortpass filter (Andover Corporation) to reduce sample heating.

After illumination, we melted the frozen samples and measured DMOB concentration using a Shimadzu HPLC (Hullar et al. 2018) with an eluent of 60:40 acetonitrile:MQ water, a flow rate of 0.70 ml min^{-1}, and detection wavelengths of 274, 273, and 287 nm for 1,2-, 1,3-, and 1,4-DMOB, respectively.

To account for differing photon fluxes across samples types and experiment days, we used 2-nitrobenzaldehyde (2NB) as a chemical actinometer (Galbavy et al. 2010, Hullar et al. 2020, Hullar et al. 2018). Except for snow samples, we prepared 10 μM 2NB actinometry samples on each experiment day using the same sample preparation and experiment treatment as the test compound illuminations, although the illumination times were shorter. For snow samples, daily j_{2NB} was determined by measuring j_{2NB} in aqueous solution and correcting by a previously determined ratio ($j_{2NB,snow}$ / $j_{2NB,aq}$ ± 1 σ = 0.38 ± 0.015), as described in earlier work (Hullar et al. 2020).

We used TUV (Madronich and Flocke 1998) to model spectral actinic fluxes for Summit, Greenland at noon on the summer solstice (subsequently referred to "Summit conditions"). We used default settings (option 1) except for wavelength interval = 0.1 nm, latitude = 72.6 degrees, ground surface elevation = 3,200 m, simulation elevation = 3,200 m, total column ozone = 308 Dobson units, surface albedo = 0.93, and four radiative transfer streams. Using methods described previously (Hullar et al. 2020), we calculated laboratory photon fluxes at 1 nm intervals from measured relative light intensities and our j_{2NB} values, then interpolated those fluxes to 0.1 nm resolution.

2.4 Determining rate constants and quantum yields for DMOB loss

We determined DMOB photodegradation rate constants using the same approach used for guaiacol and PAHs (Hullar et al. 2020, Hullar et al. 2018). We illuminated samples with simulated polar sunlight, periodically removing a beaker (and corresponding dark beaker) for analysis. To determine the photodegradation rate constant, we first calculated the natural logarithm of the ratio of the DMOB concentration at time t to the initial DMOB concentration, then adjusted these ratios by a correction factor (Supplemental Table S1) to account for differences in photon flux at each sample position (Hullar et al. 2020, Hullar et al. 2018). The linear regression slope of illuminated samples gives the pseudo-first-order rate constant for loss during illumination, j_{DMOB}; for dark controls, we get the rate constant for dark loss, $k'_{DMOB,dark}$. To calculate the net loss attributable to photodegradation, we subtracted $k'_{DMOB,dark}$ from j_{DMOB} to give the dark-corrected experimental photodegradation rate constant $j_{DMOB,exp}$. We then normalized this value for the experimental photon flux by dividing $j_{DMOB,exp}$ by the daily measured j_{2NB} value to give the photon flux-normalized photodegradation rate constant, j^*_{DMOB}. Full equations are given in our previous work [14,18].

https://doi.org/10.5194/acp-2021-875
Preprint. Discussion started: 1 November 2021


Atmospheric Chemistry and Physics Discussions

We calculated quantum yields for each DMOB using methods described previously (Hullar et al. 2020). In short, the quantum yield was determined for each DMOB by dividing the dark-corrected experimental photodegradation rate constant ($j_{DMOB,exp}$) by the measured aqueous molar absorptivity ($\varepsilon_{DMOB,\lambda}$) and the calculated photon flux in our experimental system. We determined aqueous solution molar absorptivities for each DMOB ($\varepsilon_{DMOB,\lambda}$, Supplemental Table S2) by measuring absorbance spectra in five solutions (10-1000 μM) at 25 °C using a UV-2501PC spectrophotometer (Shimadzu) in 1.0 cm cuvettes against a MQ reference cell. The calculated quantum yields are an average value over the ranges of 250-317, 250-315, and 250-341 nm for 1,2-, 1,3-, and 1,4-DMOB, respectively. We chose the low end of this range because it represents a rough natural minimum of light absorbance for the three compounds and does not have any photon flux for either Summit conditions or in our experimental system; the upper cutoff varies for each compound and is the wavelength above which the molar absorptivity is less than 5×10^{-5} M^{-1} cm^{-1}. Based on light absorption spectra for the three compounds (discussed in the results section), the wavelengths driving photodegradation in our experiments are 270-300, 270-310, and 280-310 nm for 1,2-, 1,3-, and 1,4-DMOB, respectively. We estimated molar absorptivities at the air-ice interface by applying the results of the computational modeling to the measured aqueous molar absorptivities, as described in the results section below.

2.5 Computational methods

To investigate possible shifts in light absorbance at the air-ice interface for the three dimethoxybenzene isomers, we used a multimodel approach that combines classical and first-principles molecular dynamics (FPMD) simulations, excited state calculations using time-dependent density functional theory (TDDFT), and machine learning (ML) (Bononi et al. 2020, Tibshirani 2011).

As in our recent work on phenol and guaiacol, models of DMOB in aqueous solutions and at the ice surface were equilibrated in classical MD simulations using the OPLS forcefield and the TIP4P/ice water model (Abascal et al. 2005). To model the air-ice interface we utilized an ice slab model, which captures a well-equilibrated surface structure and reproduces recent measurements for QLLs (Kling et al. 2018, Sanchez et al. 2017). We then performed FPMD simulations of the DMOB isomers in solution at 27 °C and at the air–ice interface at -10 °C. Density functional theory (DFT)-based FPMD simulations were run using the Perdew-Burke-Ernzerhof exchange and correlation functional with D3 van der Waals corrections, a double-Z valence polarizable basis set for valence states and norm-conserving pseudopotentials for the core states and the nuclei, as implemented in the CP2K code (Grimme et al. 2010, Hartwigsen et al. 1998, Perdew et al. 1996, VandeVondele et al. 2005). For each 50 ps FPMD simulation trajectory, we extracted approximately 200 statistically independent frames, replaced the explicit water molecules with the self-consistent continuum solvation scheme (Timrov et al. 2015), and finally computed absorption spectra for each frame using TDDFT as implemented in the Quantum-Espresso package (Casida et al. 2009, Giannozzi et al. 2017, Rocca et al. 2008). To account for the configurational sampling at finite temperature in the specific solvation environment, we computed the final spectra by ensemble averaging the 200 single frame calculations for each isomer (Ge et al. 2015, Timrov et al. 2016).

As a refinement to our former approach, we developed a universal ML model to predict the absorption spectra for all three DMOB isomers. To accomplish the transferability, we adopted a more sophisticated atomic descriptor - the Bispectrum Component (BC) (Bartok et al. 2013,

https://doi.org/10.5194/acp-2021-875
Preprint. Discussion started: 1 November 2021


Atmospheric Chemistry and Physics Discussions

Thompson et al. 2015). BC describes each molecule's atomic environment by projecting the weighted atomic densities to four-dimensional hyperspherical harmonics, and it has been previously applied to ML interatomic potential development and material property predictions (Cusentino et al. 2020, Legrain et al. 2017). By using BC with the least absolute shrinkage and selection operator (LASSO) regression model (Tibshirani 2011), we attain a more precise estimate of the low-energy, long-wavelength tails of the spectra, which are important for calculating rates of photon absorption since the photon flux is increasing in this region. To assess the relative contributions of the phenyl ring and methoxy groups to the light absorbance of each DMOB isomer, we decomposed the predicted peak wavelength from over ~5000 frames of each FPMD trajectory, with $\lambda_0 \approx 586$ nm fitted as the intercept of the ML model. Further details about the simulation procedures and parameters to compute BC and analysis of excitation energy predictions from the LASSO model are available Supplemental Section S1.

3. Results

3.1. Illumination experiments

As described in sections 2.2 and 2.3, we prepared samples using one of several methods designed to place the DMOB isomer into aqueous solution, LLRs, or at the air-ice interface. Then, we illuminated the samples, periodically removing them for analysis. Supplemental Figures S1 through S12 show the results for each illumination experiment, with each data point representing one sample beaker. Generally, dark controls show slight loss of DMOB, probably attributable to volatilization; illuminated samples often show considerably greater loss, presumably due to photodegradation, but the extent of loss depends on DMOB isomer and sample preparation method. Within an experiment, sample-to-sample variability was generally less for aqueous, LN2, and VD-to-snow sample types (e.g., Supplemental Figures S1c, S3b, and S5d), while frozen solution and VD-to-ice experiments showed considerable experimental noise (Supplemental Figures S2b and S4c). Previous work (Hullar and Anastasio 2016) suggests more homogeneous solute distribution in LN2 samples compared to frozen solution samples, which may explain the reduced experimental variability in LN2 samples. This reduced variability might also be due to the fact that freezing in LN2 is fast (less than 90 seconds), which reduces the time available for reactions as solutes are concentrated during freezing, while using a freezer takes much longer, typically several hours. As discussed for our previous experiments using nature-identical snow (Hullar et al. 2020), the specific surface area (SSA) for our VD-to-snow samples is much higher than in VD-to-ice samples, which should reduce aggregation and give more robust experimental results.

3.2. DMOB photodegradation for each sample preparation method

Figure 1 summarizes the experimental results for each of the three DMOBs in aqueous solution and the various frozen sample preparations. As described above, we divided each dark-corrected, measured rate constant for DMOB loss by the corresponding measured j_{2NB} value to compensate for the different photon fluxes in each experiment, then calculated the average

https://doi.org/10.5194/acp-2021-875
Preprint. Discussion started: 1 November 2021

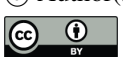

Atmospheric Chemistry and Physics Discussions

295 photon-flux-normalized rate constant (j^*_{DMOB}) for each sample treatment; error bars in Figure 1
296 are the 95% confidence interval of mean j^*_{DMOB} values.

297

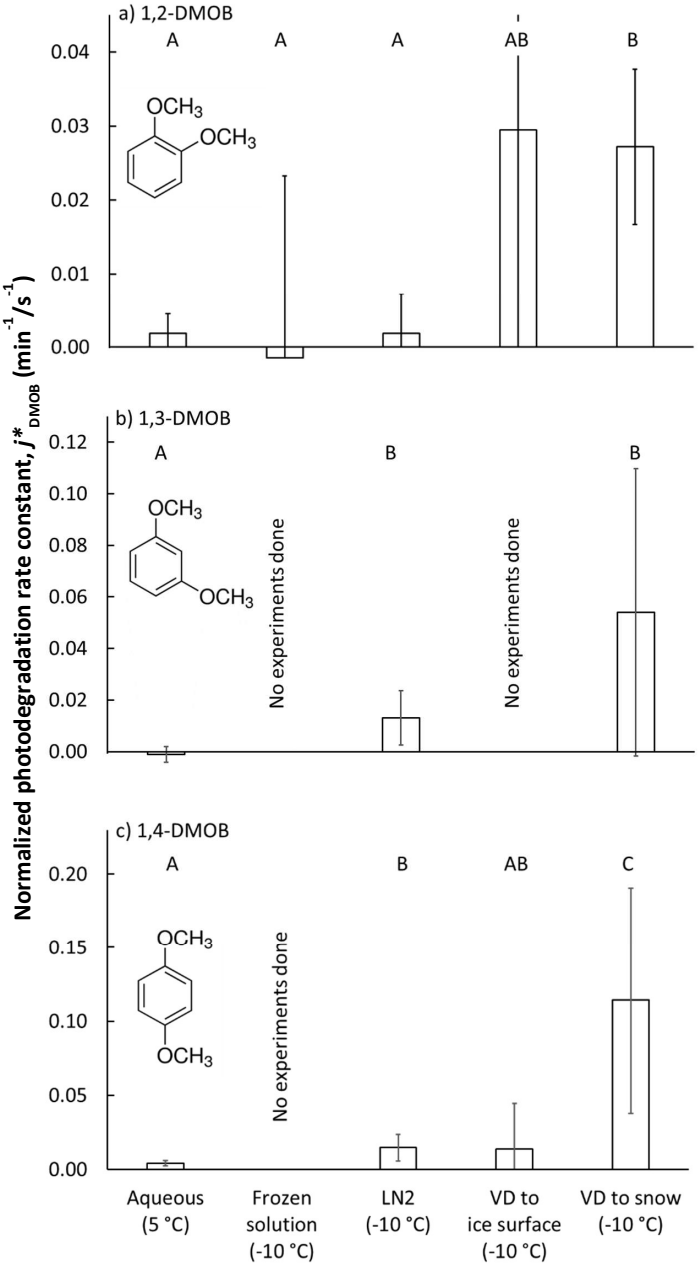

298

299

300

https://doi.org/10.5194/acp-2021-875
Preprint. Discussion started: 1 November 2021

Atmospheric Chemistry and Physics Discussions

Figure 1. Photon-flux-normalized photodegradation rate constants for each dimethoxybenzene isomer (j^*_{DMOB}) under five experimental conditions: i) aqueous solution, ii) solution frozen in a laboratory freezer ("Frozen solution"), iii) solution frozen in liquid nitrogen ("LN2"), iv) vapor-deposited DMOB to a water ice surface ("VD to ice surface"), and v) vapor-deposited DMOB to nature-identical snow ("VD to snow"). We illuminated samples at 5 °C (aqueous samples) or -10 °C (all others). Bars indicate the mean value for each sample preparation method (n = 3 - 8), with error bars as 95% upper and lower confidence limits of the mean (UCL and LCL). For each isomer, sample types having statistically indistinguishable average rate constants as determined by a Tukey-Kramer test ($P < 0.05$) are labeled with the same capital letter ("A", "B", or "C"); sample types with different letters have statistically different means.

As shown in Figure 1a, the 1,2-DMOB photodegradation rate in aqueous solution is slow and the normalized rate constant is statistically indistinguishable from zero. For frozen solution experiments, the average rate constant was negative, and the data was quite noisy. Samples frozen with liquid nitrogen ("LN2") should, like freezer-frozen samples, place solutes primarily in internal LLRs. However, the variability in 1,2-DMOB LN2 experiments is considerably less than for freezer frozen experiments, and the rate constant is roughly equivalent to that determined for aqueous solution. For both frozen solution and LN2 treatments, the rate constants are indistinguishable from zero. The two treatment methods which put 1,2-DMOB at the air-ice interface, VD to ice and VD to snow, both show normalized rate constants approximately 15 times faster than in aqueous solution or in LLRs. However, while experimental results for the VD-to-ice treatment are highly variable (with an average rate constant indistinguishable from zero), VD-to-snow experiments are more reproducible and give a normalized rate constant statistically greater than zero, showing the advantage of using nature-identical snow to study photodegradation at the air-ice interface.

1,3-DMOB results are summarized in Figure 1b. Because the frozen solution and VD-to-ice experiments were very noisy for 1,2-DMOB, we did not run experiments with these sample treatments for 1,3-DMOB. For aqueous solution, the 1,3-DMOB average rate constant is slightly negative and indistinguishable from zero. In LLRs (LN2 sample treatment), 1,3-DMOB photodegrades at a moderate rate, statistically greater than zero. Finally, at the air-ice interface (VD to snow samples), the photodegradation rate constant is approximately four times faster than in LLRs, although statistically indistinguishable from zero because of very high variability.

For 1,4-DMOB in aqueous solution (Figure 1c), the average photodegradation rate is slow, but statistically greater than zero. As with 1,3-DMOB, we did not run experiments in frozen solution for 1,4-DMOB; however, LN2 experiments, which should also place solutes primarily in LLRs, showed photodecay rates both statistically greater than zero and approximately 3-fold faster than in aqueous solution. Measured VD-to-ice rates were variable, and although the average normalized rate constant was similar to LN2, it was not statistically different than zero. As with 1,2-DMOB, the average 1,4-DMOB photodegradation rate constant at the air-ice interface (VD-to-snow experiments) is considerably faster than in either aqueous or LLR compartments, with a 26-fold enhancement relative to aqueous solution, and is statistically greater than zero.

To determine if the various sample treatment rate constants are statistically different from each other, we used the Tukey-Kramer test for multiple comparisons ($P < 0.05$) to generate statistical groupings, identified by the letters A, B, and C on Figures 1a-c. For 1,2-DMOB, mean rate constants (j^*_{DMOB}) for aqueous, frozen solution, and LN2 samples were indistinguishable from each other. However, VD to snow gave a rate constant significantly greater than these three

https://doi.org/10.5194/acp-2021-875
Preprint. Discussion started: 1 November 2021


Atmospheric Chemistry and Physics Discussions

346 sample types. Because of its high experimental variability, VD to ice could not be distinguished
347 from any of the other sample treatments. For 1,3-DMOB, aqueous samples were statistically
348 different than both LN2 and VD to snow samples. However, LN2 and VD-to-snow samples
349 could not be distinguished from each other. For 1,4-DMOB, VD-to-snow samples were
350 statistically higher than every other sample type. VD-to-ice samples were indistinguishable from
351 both aqueous and LN2 samples, although LN2 samples were statistically different, and higher,
352 than the aqueous samples.

353 Table 1 presents the rate constant enhancements for each frozen sample type relative to aqueous
354 solution; Supplemental Table S3 provides details for the various measured and computed
355 experimental parameters. For 1,2-DMOB, photodegradation proceeds at approximately the same
356 rate in LLRs and aqueous solution, but roughly 15-fold (± 9.5, 1σ) faster at the air-ice interface.
357 Because the average aqueous rate constant for 1,3-DMOB was negative, we calculated an upper-
358 bound estimate (average + 95% UCL of the mean) for the rate constant and determined
359 enhancements relative to that value. Compared to the aqueous rate constant, we estimate the 1,3-
360 DMOB rate constant in LLRs to be at least 6.9-fold faster, and at least 29-fold faster at the air-ice
361 interface. Finally, for 1,4-DMOB, enhancement in LLRs is 3.4-fold (± 2.4), and 26-fold (± 27)
362 at the air-ice interface. As noted in previous work (Hullar et al. 2020), vapor depositing a test
363 compound to nature-identical snow rather than to an ice pellet surface is more representative of
364 environmental conditions and gives more reliable experimental results, probably due to the much
365 greater SSA of the snow. Although the experimental data show considerable variability, our
366 results suggest DMOB photodegradation rate constants are somewhat faster in LLRs than in
367 corresponding aqueous solution, and considerably faster at the air-ice interface; this finding is
368 similar to previously reported results with guaiacol (Hullar et al. 2020) and several other organic
369 compounds (2007, Kahan et al. 2010, Kahan et al. 2010). Taken together with earlier work, our
370 results here suggest that at least for some compounds, aqueous solution, LLRs, and the air-ice-
371 interface can be different environments for photochemical reactivity.

372

https://doi.org/10.5194/acp-2021-875
Preprint. Discussion started: 1 November 2021

Atmospheric Chemistry and Physics Discussions

Table 1. Summary statistics for each experimental preparation method[a]

	Experimental results				Summit conditions estimates		
	n[b]	j^*_{DMOB}[c] (min^{-1}/s^{-1})	Enhancement[d] ($j^*_{DMOB,\,i} / j^*_{DMOB,\,aq}$)	Quantum Yield (Φ_{DMOB})[e] (mlc photon^{-1})	Compart-ment[g]	$j_{TUV,\,DMOB}$[h] (s^{-1})	Lifetime[i] (d)
1,2-DMOB							
Aqueous solution	3	0.0019 ± 0.0011	1	0.015 ± 0.0085	Aqueous	(5.0 ± 2.9) × 10^{-10}	23000 ± 13000
Freezer frozen solution	3	-0.0010 ± 0.0099	-0.79 ± -5.3	-0.012 ± 0.078			
Liquid nitrogen frozen solution	4	0.0019 ± 0.0030	1 ± 1.9	0.015 ± 0.027	LLR	(5.1 ± 9.0) × 10^{-10}	23000 ± 41000
Vapor-deposited to ice surface	3	0.029 ± 0.022	16 ± 15	0.13 ± 0.10			
Vapor-deposited to snow	5	0.027 ± 0.0084	15 ± 9.5	0.12 ± 0.039	QLL	(6.3 ± 1.9) × 10^{-9}	1800 ± 570
1,3-DMOB							
Aqueous solution	6	-0.0011 ± 0.0029	1[f]	< 0.016	Aqueous	< 2.6 × 10^{-10}[j]	> 45000[j]
Freezer frozen solution	0						
Liquid nitrogen frozen solution	3	0.013 ± 0.0042	> 6.9	0.11 ± 0.035	LLR	(1.8 ± 1.4) × 10^{-9}	6400 ± 5100
Vapor-deposited to ice surface	0						
Vapor-deposited to snow	5	0.054 ± 0.045	> 29	0.085 ± 0.070	QLL	(2.4 ± 2.5) × 10^{-7}	48 ± 50
1,4-DMOB							
Aqueous solution	3	0.0043 ± 0.00073	1	0.0020 ± 0.00042	Aqueous	(1.6 ± 0.34) × 10^{-7}	70 ± 14
Freezer frozen solution	0						
Liquid nitrogen frozen solution	3	0.015 ± 0.0036	3.4 ± 2.4	0.0075 ± 0.0018	LLR	(6.0 ± 1.5) × 10^{-7}	19 ± 4.7
Vapor-deposited to ice surface	5	0.014 ± 0.025	3.2 ± 6.1	0.0064 ± 0.011			
Vapor-deposited to snow	8	0.11 ± 0.091	26 ± 27	0.052 ± 0.042	QLL	(4.4 ± 3.5) × 10^{-6}	2.7 ± 2.1

[a] Samples were held at 5 °C (aqueous samples) or -10 °C (all other preparations).
[b] Number of experiments.
[c] Listed j^*_{DMOB} values (photon-flux normalized photodegradation rate constants) are means ± 1 standard deviation.

https://doi.org/10.5194/acp-2021-875
Preprint. Discussion started: 1 November 2021

Atmospheric Chemistry and Physics Discussions

[d] Enhancement factors are the ratio of the mean j^*_{DMOB} value for each preparation method to the mean aqueous j^*_{DMOB} value for that light condition, ± the propagated standard deviation.

[e] Quantum yields are calculated individually for each experiment using the measured $j_{DMOB,exp}$ and j_{2NB}. Uncertainties for quantum yields are ± 1 standard deviation.

[f] To calculate enhancement factors, we first estimated the upper bound j^*_{DMOB} value for aqueous solution as the mean + the 95% UCL, 0.00190 min^{-1}/s^{-1}. Then, we calculated enhancement factors relative to this value.

[g] For purposes of calculating $j^*_{TUV,DMOB}$ and photochemical lifetimes, quantum yields in aqueous, LLR, and QLL compartments were assumed to be represented by aqueous solution, liquid nitrogen frozen solution, and vapor-deposited to snow sample types respectively.
[h] Listed $j^*_{TUV,DMOB}$ values (calculated photodegradation rate constants for Summit, Greenland) are means ± 1 propagated standard deviation.

[i] Photochemical lifetimes are 1 / $j^*_{TUV,DMOB}$ values ± 1 propagated standard deviation.

[j] $j^*_{TUV,DMOB}$ and photochemical lifetime calculated from upper-bound estimate of 1,3-DMOB quantum yield.

373

https://doi.org/10.5194/acp-2021-875
Preprint. Discussion started: 1 November 2021

Atmospheric Chemistry and Physics Discussions

374

375 **3.3 DMOB light absorbance, quantum yields, and environmental lifetimes in solution and at**
376 **the air-ice interface**

377 Figure 2 presents the wavelength-dependent molar absorptivities for 1,2-, 1,3-, and 1,4-DMOB,
378 as well as guaiacol (which was studied in our previous work (Hullar et al. 2020)). 1,2- and 1,3-
379 DMOB in solution have nearly identical absorbance curves, with maximum absorbance at 274
380 and 273 nm, respectively. While guaiacol absorbs less strongly, its curve shape and peak
381 location are similar to 1,2- and 1,3-DMOB. In contrast, 1,4-DMOB absorbs at longer
382 wavelengths, with a peak absorbance at 287 nm. For comparison, the two black lines in Figure 2
383 show the photon flux of our experimental system (dashed line) and the modeled actinic flux for
384 Summit conditions (solid line); a more detailed graph is shown in Supplemental Figure S13.
385 While the actinic flux at Summit starts at approximately 297 nm and increases quickly with
386 increasing wavelength, the experimental flux begins earlier (roughly 280 nm) and increases more
387 gradually. 1,2- and 1,3-DMOB in solution absorb small amounts of light under our illumination
388 conditions and virtually none in the Arctic environment. In contrast, the 1,4-DMOB absorbance
389 curve has substantial overlap with both photon flux curves and therefore absorbs light under both
390 experimental and natural conditions.

391

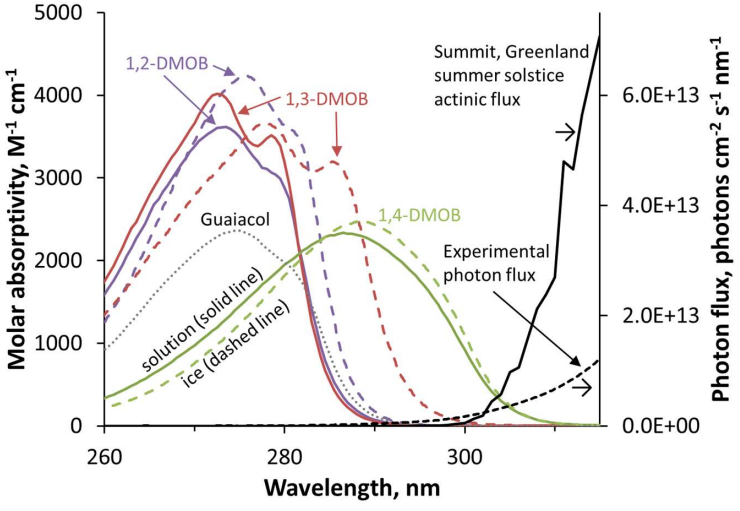

392

393

394 **Figure 2.** Light absorption spectra for the dimethoxybenzene (DMOB) isomers and guaiacol, along with
395 photon fluxes in our experiments and for Arctic summer conditions. Solid colored lines are the measured
396 molar absorptivities for each DMOB isomer, while colored dashed lines are predicted absorbance spectra
397 at the air-ice interface, estimated using the results of our molecular modeling. The solution guaiacol
398 spectrum (dotted grey line) is provided for comparison to previous work (Hullar et al. 2020). Black lines
399 (right axis) represent the modeled actinic flux for Summit conditions (solid line), and the photon flux
400 measured in our laboratory illumination system (dashed line).

https://doi.org/10.5194/acp-2021-875
Preprint. Discussion started: 1 November 2021

Atmospheric Chemistry and Physics Discussions

While we can measure light absorption by the DMOB isomers in solution, we also want to understand their absorption at the air-ice interface. To estimate this, we use molecular modeling combined with machine learning for each compound in aqueous solution and at the air-ice interface; these modeled curves are shown in Figure 3. As shown in Supplemental Figure S14, modeled absorbance bands for aqueous DMOBs peak at longer wavelengths (7 to 21 nm) compared to measurements, equal to or greater than the 7 nm difference we observed for guaiacol (Bononi et al. 2020, Hullar et al. 2020). These differences are caused by systematic underestimation in our simulations, which is a known limitation of TDDFT calculations; the peak wavelength offset relative to measured spectra tends to increase with larger molecules (Leang et al. 2012, Miura et al. 2007), consistent with the greater difference here for the DMOB isomers compared to our previous work with guaiacol. These differences can be corrected by applying the same shifts to both solution and ice spectra (Ge et al. 2015).

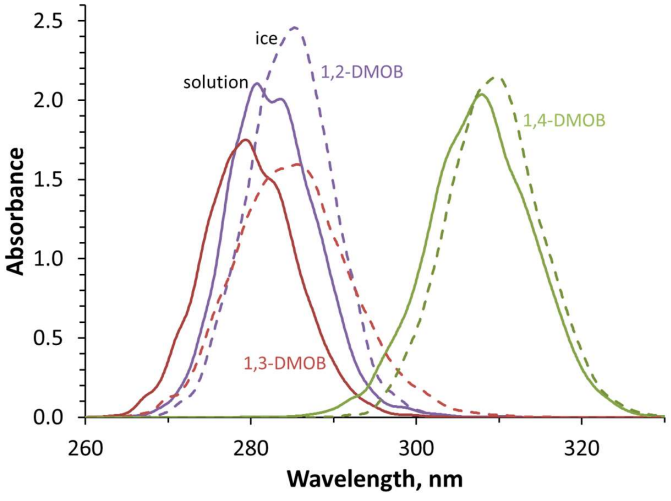

Figure 3. Modeled absorbance spectra in aqueous solution (solid lines) and at the air-ice interface (dashed lines) for each DMOB isomer. Absolute absorbance values are arbitrary, but accurately reflect the relative absorbance differences between isomers and conditions. Temperatures were 27 °C for aqueous solution and -10 °C at the air-ice interface.

While the modeling does not accurately reproduce the absolute wavelengths of absorbance, it provides useful insights into the differences between absorbance in aqueous solution and at the air-ice interface. To predict the absorbance spectrum for each DMOB at the air-ice interface, we first examine how the model predicts the absorbance changes from aqueous to air-ice interface, then apply this change to the measured aqueous spectrum. We quantify how absorbance for a given DMOB changes from aqueous to ice using three characteristics – peak location, maximum peak height, and the full width of the peak at half maximum height (FWHM). In terms of the first characteristic, all three compounds showed a bathochromic (red) shift at the air-ice interface relative to aqueous solution; shifts were 2.4, 5.2, and 1.6 nm for 1,2-, 1,3-, and 1,4-DMOB, respectively. These results are consistent with a 5-nm red shift modeled for guaiacol (Hullar et al. 2020) and previous observations of anisole showing a 4-nm red shift at the air-ice interface

https://doi.org/10.5194/acp-2021-875
Preprint. Discussion started: 1 November 2021


Atmospheric Chemistry and Physics Discussions

(Malongwe et al. 2016), but less than the 10-15 nm red shifts observed for three aniline derivatives (Corrochano et al. 2017). For peak height, modeled absorbance peaks of 1,2- and 1,4-DMOB were higher at the air-ice interface compared to in solution, by 17 and 6% respectively, while the 1,3-DMOB peak height on ice was 91% of the modeled aqueous value. In terms of peak width, 1,2- and 1,4-DMOB had narrower peaks on ice, 94 and 92% of the aqueous FWHM, respectively, while 1,3-DMOB had a 27% wider peak on ice. Using this information, we applied the modeled peak shifts, peak height changes, and FWHM differences to the measured aqueous absorbance spectrum for each compound. This results in predicted absorbance spectra at the air-ice interface for each DMOB isomer, which are shown in Figure 2 (dashed colored lines) and in Supplemental Figure S14.

We also used the molecular model results to assess the relative contributions of the phenyl ring and methoxy groups to the light absorbance of each DMOB. As indicated in Supplemental Figure S15, small geometrical changes in the phenyl ring are primarily responsible for the shifts in the absorption spectra for all three DMOB isomers, while the methoxy groups make a minor contribution. Changes in the geometry of the phenyl ring are responsible for 95 - 98% of the light absorbance shifts in aqueous solution and 96 - 98% at the air-ice interface. These findings are consistent with our previous work on guaiacol (Bononi et al. 2020, Hullar et al. 2020). Overall, these results suggest that differences in the atomic environments around the aromatic ring modify its geometry and determine their vertical excitation and are the primary factor controlling light absorption changes between aqueous solution and the air–ice interface.

As seen in Figure 2, the predicted spectrum for each isomer at the air-ice interface (dashed colored line) is noticeably different than the measured aqueous spectrum (solid colored line), with bathochromic peak shifts and changes in absorbance spectrum shape. To assess the impact of these changes on light absorbance, for each isomer we multiplied the aqueous and air-ice interface wavelength-specific molar absorptivities by the experimental or Summit photon fluxes to determine the rate constant for light absorbance at each wavelength (Supplemental Figure S16). We then summed the wavelength-specific values to obtain the overall rate constant for light absorbance in aqueous solution and at the air-ice interface, for laboratory and Summit light conditions (Supplemental Table S4). Because all three isomers show bathochromic absorbance shifts at the air-ice interface relative to aqueous solution, the overall rate constants for light absorption are generally higher at the air-ice interface. 1,3-DMOB, which has the largest absorbance spectrum bathochromic shift (5.2 nm), shows the largest change in overall light absorption, with a 5.3-fold increase relative to aqueous solution for experimental light conditions; for Summit actinic flux, the rate constant of light absorption increases by a factor of 170 from solution to air-ice interface. Conversely, the light absorption peak for 1,4-DMOB shifts only slightly from solution to ice and has a greater overlap with the photon flux curves in solution, so the rate of light absorption increases only slightly (10% or less) from solution to the air-ice interface. These results show that the amount of light absorbed can be dramatically affected by absorbance changes and that this effect depends strongly on the position of the absorbance spectrum relative to photon fluxes and on the magnitude of the absorbance shift on ice. Comparing the overall light absorbed under laboratory versus Summit light conditions, 1,2-DMOB in either aqueous solution or at the air-ice interface absorbs around 200 times as much light in our lab system compared to Summit, while for 1,4-DMOB the light absorption is approximately equal in both systems. 1,3-DMOB presents a more complex picture: in aqueous solution, the rate constant of light absorption is about 400-fold greater under laboratory

https://doi.org/10.5194/acp-2021-875
Preprint. Discussion started: 1 November 2021


Atmospheric Chemistry and Physics Discussions

illumination compared to Summit light conditions, but at the air-ice interface, light absorption is only 12-fold greater in the lab relative to Summit conditions due to the absorbance shift on ice. For 1,2- and 1,3-DMOB, wavelengths from 275 to 295 and 295 to 315 nm are most photochemically important for lab and Summit light conditions, respectively; for 1,4-DMOB, these ranges are 280-315 and 300-320 nm.

Our observed increases in photochemical degradation rates at the air-ice interface can be caused by increases in light absorbance, quantum yield, or a combination of both. As shown previously (Hullar et al. 2020), by solving equation (1) for quantum yield we can use the calculated enhancements in the rate constant of light absorbance from our modeling results to estimate how quantum yields change from solution to the air-ice interface. Using the measured aqueous and predicted ice spectra for each compound, we calculated the quantum yields for each isomer under various conditions (Table 1). Our experimental results suggest LLRs may represent an environment different from either aqueous solution or QLLs. However, we did not model light absorbance changes in LLRs, so for the quantum yield calculations we assumed our test compounds have the same molar absorptivities in LLRs as in aqueous solution.

For 1,2-DMOB, the quantum yield in aqueous solution is 0.015 (± 0.0085, 1 σ). Because the experimental data is noisy, the calculated quantum yield for frozen solution is statistically indistinguishable from zero. LN2 samples had a similar quantum yield to aqueous solution, although again the quantum yield is indistinguishable from zero. In both VD-to-ice and VD-to-snow samples, where we would expect to find 1,2-DMOB at the air-ice interface, the quantum yields were approximately 8 times higher than in aqueous solution or LLRs, and were the highest calculated for any isomer and sample type, e.g., 0.12 ± 0.039 in the VD-to-snow samples. For 1,3-DMOB, the negative experimental reaction rate constant in solution (Figure 1b) precludes calculating a quantum yield; however, using the calculated confidence interval (Table 1) we can provide an upper-bound estimate of 0.016. In both LN2 (LLR) and VD-to-snow (air-ice interface) sample types, the 1,3-DMOB quantum yields are similar, and at least 5 times higher than in aqueous solution. For 1,4-DMOB, the aqueous solution quantum yield of 0.0020 (± 0.00042) is approximately 8-fold less than that of 1,2-DMOB; the quantum yield in LLRs is approximately 4 times higher than in aqueous solution. At the air-ice interface, the 1,4-DMOB quantum yield (0.052 ± 0.042 mlc photon^{-1}) had the largest increase in quantum yield relative to aqueous solution of any of the isomers, approximately 26-fold. These results are in the same range as previous results showing 40- and 3-fold increases in air-ice interface quantum yields for guaiacol and nitrate, respectively (Hullar et al. 2020, 2018).

Next, we evaluated the relative contributions of increased light absorbance and larger quantum yields to the photodegradation rate enhancements at the air-ice interface relative to solution. For 1,2- and 1,4-dimethoxybenzene, the faster photodegradation on ice is primarily due to an increase in quantum yield. In contrast, for 1,3-DMOB the enhanced photodegradation at the air-ice interface is roughly equally due to increases in quantum yield and light absorbance. As in our earlier work with guaiacol (Hullar et al. 2020), light absorbance changes are never the dominant factor controlling rate constant enhancements. Increased light absorption accounts for 16%, 49% or less, and 4% of the reactivity enhancement on snow relative to aqueous solution for 1,2-, 1,3-, and 1,4-DMOB, respectively. Thus, higher quantum yields account for the bulk of the enhancement seen at the air-ice interface, accounting for 84%, at least 51%, and 96% of the observed enhancements, respectively. These results are roughly consistent with our previous observations for guaiacol, where the quantum yield increased at the air-ice interface by a factor

https://doi.org/10.5194/acp-2021-875
Preprint. Discussion started: 1 November 2021


Atmospheric Chemistry and Physics Discussions

of 41, accounting for 95% of the overall 77-fold increase in reactivity compared to aqueous solution (Hullar et al. 2020).

3.4 Estimated photodegradation rate constants under environmental conditions and sensitivity to absorbance shifts

To assess the environmental significance of our findings, we calculated dimethoxybenzene photodegradation rate constants and photochemical lifetimes in each compartment for Summit, Greenland conditions (Table 1). For these calculations, we used modeled actinic fluxes at Summit (section 2.3) and our estimated quantum yields (section 3.3); because our computational modeling did not include LLRs, we used measured aqueous spectra to represent absorbance in both aqueous and LLR compartments, and our predicted ice spectra (Figure 2) for the air-ice interface. 1,2-DMOB has slow photodegradation rate constants and very long photochemical lifetimes (~60 years) in solution and in LLRs. At the air-ice interface, it photodegrades 13 times faster, but the resulting lifetime is still long – approximately 1800 days of midday, summer solstice sunlight. Thus even with the rate constant enhancement at the interface, direct photochemical degradation is still apparently negligible. Similar to 1,2-DMOB, 1,3-DMOB has long lifetimes and slow degradation rate constants in the aqueous and LLR compartments (Table 1). However, because of its significant bathochromic absorbance shift (5.2 nm), the lifetime of 1,3-DMOB at the air-ice interface decreases to 48 days, suggesting its persistence in the environment may change significantly depending on where it is found in snow or ice. For 1,4-DMOB, its absorption is already at longer wavelengths compared to the other two isomers, so it absorbs more light under environmental conditions and therefore can undergo faster photodegradation: lifetimes are 70, 19, and 2.7 days in aqueous solution, LLRs, and QLLs, respectively, under Summit conditions. These results show that the location of an impurity in a snowpack can strongly influence photochemical degradation rates. For compounds that absorb sunlight substantially in solution, direct photochemical reactions at the air-ice interface may be an important transformation process in snowpacks. However, quantifying this effect requires understanding the portion of a compound at the air-ice interface, which is poorly known.

As discussed above, enhanced reactivity at the air-ice interface is primarily due to increases in the quantum yield, ranging from at least 5-fold (1,3-DMOB) to 41-fold (guaiacol) (Hullar et al. 2020). However, although we can predict absorbance shifts at the air-ice interface using molecular modeling techniques, we cannot currently predict quantum yield changes using either computational or experimental methods. While changes in quantum yields affect photodegradation rate constants linearly – a doubling of quantum yield will double the rate constant – absorbance shifts cause nonlinear effects. To evaluate the impact of absorbance shifts on compound photodegradation, Figure 4a shows the calculated ratios of absorbance-shifted rate constants to the unshifted rate constant. We estimated environmental ($j_{TUV,DMOB}$) and lab photodegradation rate constants for each isomer using our calculated aqueous solution quantum yield, Summit or experimental photon fluxes, and our measured aqueous absorbance including bathochromic and hypsochromic shifts to simulate absorbance changes in/on ice. For our experimental photon flux, a 5 nm bathochromic shift (approximately equal to the largest shift modeled for the three DMOB isomers) changes the photodegradation rate constants by factors of 3.1 and 2.1 for 1,2-DMOB and 1,4-DMOB respectively. A 10 nm shift, similar to that measured for several aniline derivatives (Corrochano et al. 2017), increases the photodegradation rate constants by factors of 7.8 and 4.2. Because 1,4-DMOB absorbs more strongly at longer wavelengths than 1,2-DMOB and therefore has greater initial overlap with the experimental

https://doi.org/10.5194/acp-2021-875
Preprint. Discussion started: 1 November 2021

Atmospheric Chemistry and Physics Discussions

photon flux (Figure 2), shifts have a smaller impact than for 1,2-DMOB. For a 5 nm hypsochromic (blue) shift, 1,2-DMOB and 1,4-DMOB rate constants are reduced by factors of 0.24 and 0.46, respectively; for a 10 nm shift, the factors are 0.040 and 0.19. As with red shifts, 1,2-DMOB shows greater sensitivity to a blue shift than does 1,4-DMOB. With Summit actinic fluxes, we see a similar pattern, but a greater sensitivity to shift (Figure 4a) due to the faster increase in actinic flux with increasing wavelength for Summit compared to our experimental photon fluxes (Figure 2). For 1,2-DMOB, a 10 nm red or blue shift changes the rate constants by factors of 90 or 0.0078, respectively, under Summit (TUV) photon fluxes. For 1,4-DMOB, the same shifts yield changes of 16- or 0.029-fold. 1,3-DMOB has a very similar absorbance spectrum to 1,2-DMOB, and thus shows similar impacts of a shift in its absorbance spectrum (Supplemental Figure S17). Supplemental Figure S18 compares guaiacol photodegradation rate constant changes estimated using TUV actinic flux and under three different experimental light source conditions from this and previous work (Hullar et al. 2020), showing how our experimental illumination system has been improved over time, but still does not fully reproduce the solar spectrum of Summit conditions.

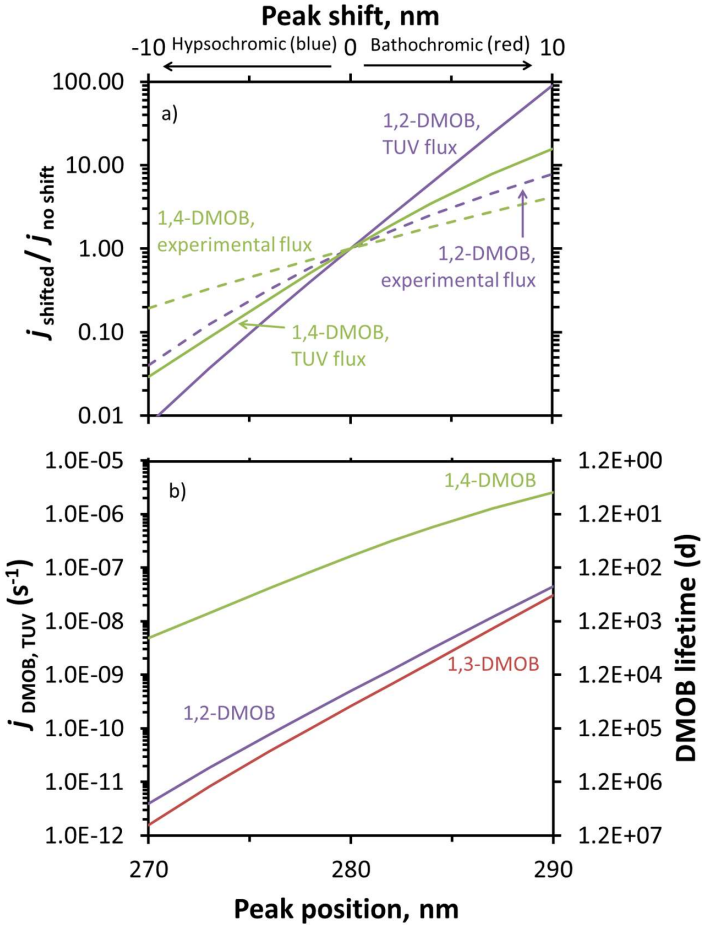

https://doi.org/10.5194/acp-2021-875
Preprint. Discussion started: 1 November 2021


Atmospheric Chemistry and Physics Discussions

583 **Figure 4**. Predicted changes to photodegradation rate constants and lifetimes resulting from absorbance
584 shifts for DMOB isomers. Rate constants were determined using calculated aqueous quantum yields,
585 aqueous absorbance spectra shifted either hypsochromically (towards shorter wavelengths) or
586 bathochromically (towards longer wavelengths), and either experimental photon fluxes (dashed lines) or
587 the modeled actinic flux for Summit conditions (solid lines). a) Changes in absorbance-shifted
588 photodegradation rate constants (j^*_{DMOB} for experimental conditions, $j^*_{DMOB,TUV}$ for TUV-modeled photon
589 fluxes) relative to unshifted values for 1,2- and 1,4-DMOB in aqueous solution. b) Estimated changes in
590 direct photodegradation rate constant ($j_{DMOB,TUV}$) and corresponding lifetime for each DMOB isomer
591 under Summit conditions for various shifts in the light absorbance peak.

592

593 While the impact of a red-shift in absorbance can be dramatic, this does not necessarily translate
594 to a short lifetime. For example, a 10-nm red shift for 1,2-DMOB increases the rate constant for
595 photodegradation by a factor of 90 (Figure 4a), but this only reduces the lifetime from 23,000 to
596 260 days (Figure 4b). 1,3-DMOB, which has essentially the same absorbance spectrum, behaves
597 similarly (Figures 4, 5, and S17). The behavior of 1,4-DMOB is different, however, since it
598 overlaps the most with the solar spectrum (Figure 2): while its rate constant for loss is less
599 sensitive to a shift in absorbance (e.g., increasing by a factor of 16 for a 10-nm red shift), this
600 changes the lifetime from 71 to 4.5 days (Figure 4b), which is short enough to be significant for
601 its environmental fate.

602 **3.5 Sensitivity analysis of absorbance parameters on photodegradation rate constants for a**
603 **hypothetical model compound**

604 To generalize our experimental findings to other chemicals, we calculated photodegradation rate
605 constants and lifetimes for a hypothetical model compound with an assumed Gaussian
606 absorbance spectrum under Summit conditions and with a quantum yield of 1. We first chose a
607 single hypothetical absorbance curve, then evaluated the impact of three variables: peak position,
608 peak width, and peak height. We created a single hypothetical model compound with
609 absorbance represented as a Gaussian curve with its peak at 280 nm, peak height (molar
610 absorptivity) of 3000 M^{-1} cm^{-1}, and a standard deviation (controlling peak width) of 7 nm. These
611 parameters were determined by fitting two Gaussian curves to the absorbance spectra for 1,2-
612 and 1,4-DMOB (Supplemental Figure S19); because the right-hand (red side) of each absorbance
613 spectrum determines the amount of light absorbed, we selected curves to fit this portion of the
614 measured absorbance spectra, then applied the average parameters to give the absorption
615 spectrum of the hypothetical compound.

616 We then evaluated the impacts of shifting the peak position widely, by ± 20 nm, as illustrated in
617 Figure S20. As shown in Figure 5a for Summit sunlight, the impact of a shift depends on the
618 where it occurs, with the rate constant for photodegradation more sensitive at shorter
619 wavelengths. For example, hypsochromically moving a peak from 280 to 260 nm decreases the
620 rate constant by a factor of 320,000, while bathochromically moving the peak from 280 to 300
621 nm leads to a 920-fold increase in rate constant. This difference is because the red shift moves
622 the absorbance spectrum towards wavelengths where some light is already being absorbed.
623 However, as discussed earlier, large increases in a rate constant do not necessarily translate to
624 significant photochemistry: lifetimes for our hypothetical compound are 2,200,000, 6.7, and
625 0.0072 days when the peak is centered at 260, 280, and 300 nm, respectively (Figure 5b). This

https://doi.org/10.5194/acp-2021-875
Preprint. Discussion started: 1 November 2021

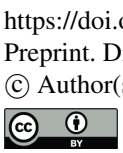

Atmospheric Chemistry and Physics Discussions

626 sensitivity of shift impact to starting peak wavelength is shown even more clearly if we consider
627 a wider wavelength range, as shown in Figure S21. Once the compound absorbance begins to
628 significantly overlap with the actinic flux curve, additional red-shifting does not dramatically
629 increase the amount of light absorbed, slowing the rate of j_{max} increase. If we assume our
630 hypothetical compound experiences a 5 nm shift, the largest shift estimated by our calculations
631 of the three DMOB isomers, the rate constant would decrease by a factor of 0.0075 for a blue
632 shift and increase by 9.2-fold for a red shift.

633

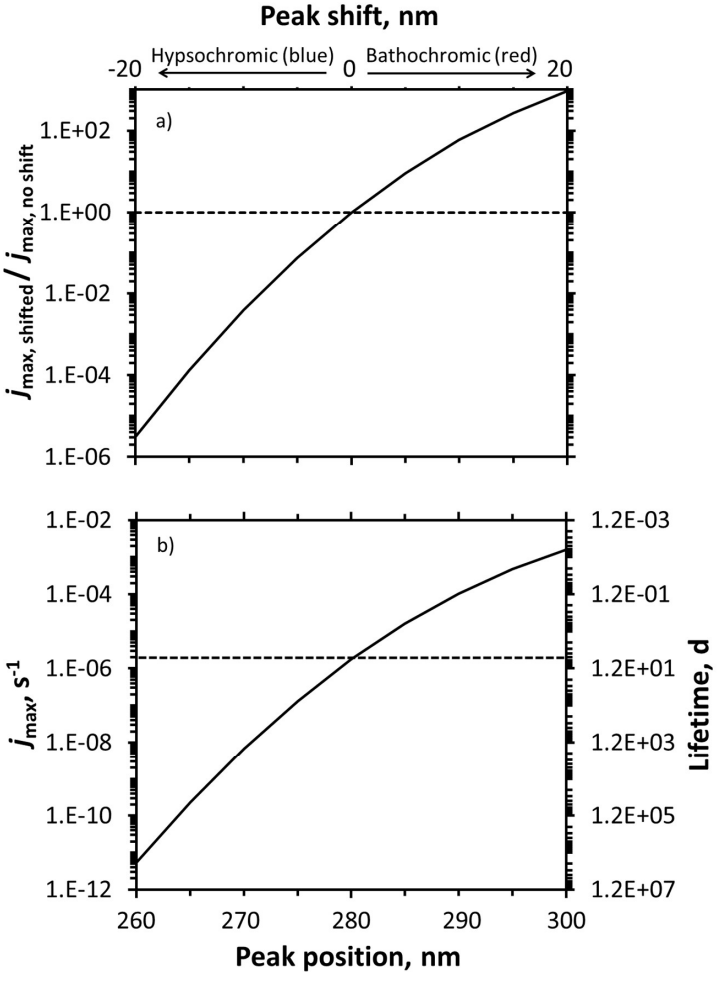

634

635 **Figure 5.** Predicted changes to photodegradation rate constants (j_{max}) and lifetimes resulting from
636 absorbance shifts for a hypothetical model compound. Rate constants (j_{max}) and lifetimes calculated using
637 an assumed quantum yield of 1, modeled actinic flux for Summit conditions, and an assumed Gaussian
638 absorbance spectrum (peak molar absorptivity 3000 M^{-1} cm^{-1}, standard deviation of 7 nm) with varying
639 peak positions. a) Ratio of shifted to unshifted j_{max} for varying hypsochromic (blue) or bathochromic

https://doi.org/10.5194/acp-2021-875
Preprint. Discussion started: 1 November 2021


Atmospheric Chemistry and Physics Discussions

(red) absorbance shifts. b) Calculated rate constants (j_{max}) and lifetimes at various peak positions. The horizontal lines intersect the curves at the baseline peak position of 280 nm.

Next, we examined the impact of peak width, as illustrated in Figure S22. From our modeling, the largest peak width change was approximately 2 nm (for 1,3-DMOB). As seen in Supplemental Figure S23, narrowing the hypothetical peak from 7 to 5 nm reduces j_{max} and increases the lifetime by 88-fold, roughly 7 times larger than the lifetime decrease caused by a 5 nm hypsochromic shift of the original 7 nm wide peak. While broadening the peak to 9 nm does increase j_{max} and decrease the lifetime, the magnitude of the change is not as significant, approximately 13-fold. Similarly to the pattern seen for peak location shifts, changes in peak width cause greater impacts when the compound's absorbance peak is located at shorter wavelengths.

Finally, we evaluated the impact of changing the peak height (hyper- and hypochromic shifts). Figure S24 shows the spectra tested, and Figure S25 the results; for comparison, our largest modeled peak height change was 17%, for 1,2-DMOB. Because the area of a Gaussian curve is proportional to its peak height, doubling the height doubles the area and therefore the light absorbed would double as well. However, compared to the impact of peak location and width, even a peak height doubling exerts a relatively small influence on peak area and therefore light absorbed. To evaluate the relative impact of absorbance shifts, broadenings, and peak height (molar absorptivity) changes on photodegradation, we assumed the largest modeled absorbance changes between aqueous solution and at the air-ice interface for the three DMOB isomers are typical for chemicals in the environment. Based on this assumption and applying these changes to our hypothetical peak, peak location and width changes at the air-ice interface probably control overall differences in light absorption, while changes in peak height likely make a minor contribution.

4 Conclusions

Our results, together with previous studies (Hullar et al. 2020, 2007, Kahan et al. 2010, Kahan et al. 2010), suggest that for some organic compounds, QLLs and LLRs represent different photochemical reaction environments that are distinct from aqueous solution. While molecular modeling and laboratory measurements have both found evidence of absorbance shifts (Corrochano et al. 2017, Heger et al. 2005, Hullar et al. 2020, Malongwe et al. 2016), our results indicate that increases in quantum yield are the major reason for enhanced photochemical reactivity at the air-ice interface. For compounds absorbing appreciable amounts of sunlight in aqueous solution, QLL and LLR reactivity increases may cause environmentally significant changes in direct photoreaction rates and lifetimes, but for chemicals that absorb very little or no sunlight, these changes do not appear to make direct photochemistry a significant sink.

Our ability to make statistically significant conclusions depended on the choice of the experimental treatment; samples frozen in liquid nitrogen or vapor deposited to nature-identical snow provided useful insights into LLR and QLL compartments, respectively. In contrast, samples frozen in a laboratory freezer or vapor deposited to a water ice surface gave results that were noisier and less valuable. In addition, computational methods allowed us to determine absorbance spectra at the air-ice interface, where experimental observations would have been difficult.

https://doi.org/10.5194/acp-2021-875
Preprint. Discussion started: 1 November 2021

Atmospheric Chemistry and Physics Discussions

683

684

685

686 **Acknowledgments**

687 We thank the National Science Foundation for funding (CHE 1806210 and AGS-PRF 1524857).
688 Calculations were performed using the Extreme Science and Engineering Discovery
689 Environment (XSEDE),87 which is supported by the National Science Foundation, grant number
690 ACI-154856

https://doi.org/10.5194/acp-2021-875
Preprint. Discussion started: 1 November 2021

Atmospheric Chemistry and Physics Discussions

5. References

Abascal, J. L. F., E. Sanz, R. G. Fernandez and C. Vega: A potential model for the study of ices and amorphous water: TIP4P/Ice, Journal of Chemical Physics, 122(23), doi: 10.1063/1.1931662, 2005.

Amaine, L., C. Guillara, N. Serpone and P. Pichat: Water treatment: Degradation of dimethoxybenzenes by the titanium dioxide-UV combination, Journal of Environmental Science and Health . Part A: Environmental Science and Engineering and Toxicology, 28(6), 1393-1408, doi: 10.1080/10934529309375949, 1993.

Barret, M., F. Domine, S. Houdier, J. C. Gallet, P. Weibring, J. Walega, A. Fried and D. Richter: Formaldehyde in the Alaskan Arctic snowpack: Partitioning and physical processes involved in air-snow exchanges, Journal of Geophysical Research-Atmospheres, 116, doi: 10.1029/2011jd016038, 2011.

Bartels-Rausch, T., H. W. Jacobi, T. F. Kahan, J. L. Thomas, E. S. Thomson, J. P. D. Abbatt, M. Ammann, J. R. Blackford, H. Bluhm, C. Boxe, F. Domine, M. M. Frey, I. Gladich, M. I. Guzman, D. Heger, T. Huthwelker, P. Klan, W. F. Kuhs, M. H. Kuo, S. Maus, S. G. Moussa, V. F. McNeill, J. T. Newberg, J. B. C. Pettersson, M. Roeselova and J. R. Sodeau: A review of air-ice chemical and physical interactions (AICI): liquids, quasi-liquids, and solids in snow, Atmospheric Chemistry and Physics, 14(3), 1587-1633, doi: 10.5194/acp-14-1587-2014, 2014.

Bartok, A. P., R. Kondor and G. Csanyi: On representing chemical environments, Physical Review B, 87(18), 16, doi: 10.1103/PhysRevB.87.184115, 2013.

Bononi, F. C., Z. K. Chen, D. Rocca, O. Andreussi, T. Hullar, C. Anastasio and D. Donadio: Bathochromic Shift in the UV-Visible Absorption Spectra of Phenols at Ice Surfaces: Insights from First-Principles Calculations, Journal of Physical Chemistry A, 124(44), 9288-9298, doi: 10.1021/acs.jpca.0c07038, 2020.

Casida, M. E., H. Chermette and D. Jacquemin: Time-dependent density-functional theory for molecules and molecular solids Preface, Journal of Molecular Structure-Theochem, 914(1-3), 1-2, doi: 10.1016/j.theochem.2009.08.013, 2009.

Chu, L. and C. Anastasio: Quantum yields of hydroxyl radical and nitrogen dioxide from the photolysis of nitrate on ice, Journal of Physical Chemistry A, 107(45), 9594-9602, doi: 10.1021/jp0349132, 2003.

Chu, L. and C. Anastasio: Formation of hydroxyl radical from the photolysis of frozen hydrogen peroxide, Journal of Physical Chemistry A, 109(28), 6264-6271, doi: 10.1021/jp051415f, 2005.

Chu, L. and C. Anastasio: Temperature and wavelength dependence of nitrite photolysis in frozen and aqueous solutions, Environmental Science & Technology, 41(10), 3626-3632, doi: 10.1021/es062731q, 2007.

732 Corrochano, P., D. Nachtigallová and P. Klán: Photooxidation of Aniline Derivatives Can Be Activated by
733 Freezing Their Aqueous Solutions, Environmental Science & Technology, 51(23), 13763-13770, doi:
734 10.1021/acs.est.7b04510, 2017.

735
736 Cusentino, M. A., M. A. Wood and A. P. Thompson: Explicit Multielement Extension of the Spectral
737 Neighbor Analysis Potential for Chemically Complex Systems, Journal of Physical Chemistry A, 124(26),
738 5456-5464, doi: 10.1021/acs.jpca.0c02450, 2020.

739
740 Domine, F. and P. B. Shepson: Air-snow interactions and atmospheric chemistry, Science, 297(5586),
741 1506-1510, 2002.

742
743 France, J. L., M. D. King, M. M. Frey, J. Erbland, G. Picard, S. Preunkert, A. MacArthur and J. Savarino:
744 Snow optical properties at Dome C (Concordia), Antarctica; implications for snow emissions and snow
745 chemistry of reactive nitrogen, Atmospheric Chemistry and Physics, 11(18), 9787-9801, doi:
746 10.5194/acp-11-9787-2011, 2011.

747
748 Galbavy, E. S., C. Anastasio, B. L. Lefer and S. R. Hall: Light penetration in the snowpack at Summit,
749 Greenland: Part 1 Nitrite and hydrogen peroxide photolysis, Atmospheric Environment, 41(24), 5077-
750 5090, doi: 10.1016/j.atmosenv.2006.04.072, 2007.

751
752 Galbavy, E. S., K. Ram and C. Anastasio: 2-Nitrobenzaldehyde as a chemical actinometer for solution and
753 ice photochemistry, Journal of Photochemistry and Photobiology a-Chemistry, 209(2-3), 186-192, doi:
754 10.1016/j.jphotochem.2009.11.013, 2010.

755
756 Ge, X. C., I. Timrov, S. Binnie, A. Biancardi, A. Calzolari and S. Baroni: Accurate and Inexpensive
757 Prediction of the Color Optical Properties of Anthocyanins in Solution, Journal of Physical Chemistry A,
758 119(16), 3816-3822, doi: 10.1021/acs.jpca.5b01272, 2015.

759
760 Giannozzi, P., O. Andreussi, T. Brumme, O. Bunau, M. B. Nardelli, M. Calandra, R. Car, C. Cavazzoni, D.
761 Ceresoli, M. Cococcioni, N. Colonna, I. Carnimeo, A. Dal Corso, S. de Gironcoli, P. Delugas, R. A. DiStasio,
762 A. Ferretti, A. Floris, G. Fratesi, G. Fugallo, R. Gebauer, U. Gerstmann, F. Giustino, T. Gorni, J. Jia, M.
763 Kawamura, H. Y. Ko, A. Kokalj, E. Kucukbenli, M. Lazzeri, M. Marsili, N. Marzari, F. Mauri, N. L. Nguyen, H.
764 V. Nguyen, A. Otero-de-la-Roza, L. Paulatto, S. Ponce, D. Rocca, R. Sabatini, B. Santra, M. Schlipf, A. P.
765 Seitsonen, A. Smogunov, I. Timrov, T. Thonhauser, P. Umari, N. Vast, X. Wu and S. Baroni: Advanced
766 capabilities for materials modelling with QUANTUM ESPRESSO, Journal of Physics-Condensed Matter,
767 29(46), 30, doi: 10.1088/1361-648X/aa8f79, 2017.

768
769 Grannas, A. M., W. C. Hockaday, P. G. Hatcher, L. G. Thompson and E. Mosley-Thompson: New
770 revelations on the nature of organic matter in ice cores, Journal of Geophysical Research-Atmospheres,
771 111(D4), doi: D04304 10.1029/2005jd006251, 2006.

772

https://doi.org/10.5194/acp-2021-875
Preprint. Discussion started: 1 November 2021

Atmospheric Chemistry and Physics Discussions

773 Grannas, A. M., A. E. Jones, J. Dibb, M. Ammann, C. Anastasio, H. J. Beine, M. Bergin, J. Bottenheim, C. S.
774 Boxe, G. Carver, G. Chen, J. H. Crawford, F. Domine, M. M. Frey, M. I. Guzman, D. E. Heard, D. Helmig, M.
775 R. Hoffmann, R. E. Honrath, L. G. Huey, M. Hutterli, H. W. Jacobi, P. Klan, B. Lefer, J. McConnell, J. Plane,
776 R. Sander, J. Savarino, P. B. Shepson, W. R. Simpson, J. R. Sodeau, R. von Glasow, R. Weller, E. W. Wolff
777 and T. Zhu: An overview of snow photochemistry: evidence, mechanisms and impacts, Atmospheric
778 Chemistry and Physics, 7(16), 4329-4373, 2007.

779
780 Grimme, S., J. Antony, S. Ehrlich and H. Krieg: A consistent and accurate ab initio parametrization of
781 density functional dispersion correction (DFT-D) for the 94 elements H-Pu, Journal of Chemical Physics,
782 132(15), 19, doi: 10.1063/1.3382344, 2010.

783
784 Hartwigsen, C., S. Goedecker and J. Hutter: Relativistic separable dual-space Gaussian pseudopotentials
785 from H to Rn, Physical Review B, 58(7), 3641-3662, doi: 10.1103/PhysRevB.58.3641, 1998.

786
787 Heger, D., J. Jirkovsky and P. Klán: Aggregation of methylene blue in frozen aqueous solutions studied by
788 absorption spectroscopy, Journal of Physical Chemistry A, 109(30), 6702-6709, doi: 10.1021/jp050439j,
789 2005.

790
791 Hullar, T. and C. Anastasio: Direct visualization of solute locations in laboratory ice samples, Cryosphere,
792 10(5), 2057-2068, doi: 10.5194/tc-10-2057-2016, 2016.

793
794 Hullar, T., F. C. Bononi, Z. K. Chen, D. Magadia, O. Palmer, T. Tran, D. Rocca, O. Andreussi, D. Donadio
795 and C. Anastasio: Photodecay of guaiacol is faster in ice, and even more rapid on ice, than in aqueous
796 solution, Environmental Science-Processes & Impacts, 22(8), 1666-1677, doi: 10.1039/d0em00242a,
797 2020.

798
799 Hullar, T., D. Magadia and C. Anastasio: Photodegradation Rate Constants for Anthracene and Pyrene
800 Are Similar in/on Ice and in Aqueous Solution, Environmental Science & Technology, 52(21), 12225-
801 12234, doi: 10.1021/acs.est.8b02350, 2018.

802
803 Jacobi, H. W., R. C. Bales, R. E. Honrath, M. C. Peterson, J. E. Dibb, A. L. Swanson and M. R. Albert:
804 Reactive trace gases measured in the interstitial air of surface snow at Summit, Greenland, Atmospheric
805 Environment, 38(12), 1687-1697, doi: 10.1016/j.atmosenv.2004.01.004, 2004.

806
807 Kahan, T. F. and D. J. Donaldson: Photolysis of polycyclic aromatic hydrocarbons on water and ice
808 surfaces, Journal of Physical Chemistry A, 111(7), 1277-1285, doi: 10.1021/jp066660t, 2007.

809
810 Kahan, T. F. and D. J. Donaldson: Benzene photolysis on ice: Implications for the fate of organic
811 contaminants in the winter, Environmental Science & Technology, 44(10), 3819-3824, doi:
812 10.1021/es100448h, 2010.

813

814 Kahan, T. F., N. O. A. Kwamena and D. J. Donaldson: Different photolysis kinetics at the surface of frozen
815 freshwater vs. frozen salt solutions, Atmospheric Chemistry and Physics, 10(22), 10917-10922, doi:
816 10.5194/acp-10-10917-2010, 2010.

817
818 Kahan, T. F., R. Zhao, K. B. Jumaa and D. J. Donaldson: Anthracene photolysis in aqueous solution and
819 ice: Photon flux dependence and comparison of kinetics in bulk ice and at the air-ice interface,
820 Environmental Science & Technology, 44(4), 1302-1306, doi: 10.1021/es9031612, 2010.

821
822 Kania, R., J. K. Malongwe, D. Nachtigallová, J. Krausko, I. Gladich, M. Roeselová, D. Heger and P. Klán:
823 Spectroscopic properties of benzene at the air-ice interface: A combined experimental-computational
824 approach, Journal of Physical Chemistry A, 118(35), 7535-7547, doi: 10.1021/jp501094n, 2014.

825
826 Kling, T., F. Kling and D. Donadio: Structure and Dynamics of the Quasi-Liquid Layer at the Surface of Ice
827 from Molecular Simulations, Journal of Physical Chemistry C, 122(43), 24780-24787, doi:
828 10.1021/acs.jpcc.8b07724, 2018.

829
830 Krausko, J., J. K. Malongwe, G. Bičanová, P. Klán, D. Nachtigallová and D. Heger: Spectroscopic properties
831 of naphthalene on the surface of ice grains revisited: A combined experimental computational
832 approach, Journal of Physical Chemistry A, 119(32), 8565-8578, doi: 10.1021/acs.jpca.5b00941, 2015.

833
834 Leang, S. S., F. Zahariev and M. S. Gordon: Benchmarking the performance of time-dependent density
835 functional methods, Journal of Chemical Physics, 136(10), 12, doi: 10.1063/1.3689445, 2012.

836
837 Legrain, F., J. Carrete, A. van Roekeghem, S. Curtarolo and N. Mingo: How Chemical Composition Alone
838 Can Predict Vibrational Free Energies and Entropies of Solids, Chemistry of Materials, 29(15), 6220-6227,
839 doi: 10.1021/acs.chemmater.7b00789, 2017.

840
841 Madronich, S. and S. J. Flocke (1998). The role of solar radiation in atmospheric chemistry. Handbook of
842 Environmental Chemistry. P. Boule. Heidelberg, Springer: 1-26.

843
844 Malongwe, J. K., D. Nachtigallová, P. Corrochano and P. Klán: Spectroscopic properties of anisole at the
845 air-ice interface: A combined experimental-computational approach, Langmuir, 32(23), 5755-5764, doi:
846 10.1021/acs.langmuir.6b01187, 2016.

847
848 Matykiewiczová, N., R. Kurkova, J. Klanova and P. Klán: Photochemically induced nitration and
849 hydroxylation of organic aromatic compounds in the presence of nitrate or nitrite in ice, Journal of
850 Photochemistry and Photobiology a-Chemistry, 187(1), 24-32, 2007.

851
852 McFall, A. S. and C. Anastasio: Photon flux dependence on solute environment in water ices,
853 Environmental Chemistry, 13(4), 682-687, doi: http://dx.doi.org/10.1071/EN15199, 2016.

854

855 McFall, A. S., K. C. Edwards and C. Anastasio: Nitrate Photochemistry at the Air-Ice Interface and in Other
856 Ice Reservoirs, Environmental Science & Technology, 52(10), 5710-5717, doi: 10.1021/j.acs.est.8b00095,
857 2018.

858
859 Miura, M., Y. Aoki and B. Champagne: Assessment of Time-Dependent Density-Functional Schemes for
860 Computing the Oscillator Strengths of Benzene, Phenol, Aniline, and Fluorobenzene, J. Chem. Phys., 127,
861 084103- 084117, doi: 10.1063/1.2761886, 2007.

862
863 Perdew, J. P., K. Burke and M. Ernzerhof: Generalized gradient approximation made simple, Physical
864 Review Letters, 77(18), 3865-3868, doi: 10.1103/PhysRevLett.77.3865, 1996.

865
866 Phillips, G. J. and W. R. Simpson: Verification of snowpack radiation transfer models using actinometry,
867 Journal of Geophysical Research-Atmospheres, 110(D8), doi: D08306 10.1029/2004jd005552, 2005.

868
869 Ram, K. and C. Anastasio: Photochemistry of phenanthrene, pyrene, and fluoranthene in ice and snow,
870 Atmospheric Environment, 43(14), 2252-2259, doi: 10.1016/j.atmosenv.2009.01.044, 2009.

871
872 Rocca, D., R. Gebauer, Y. Saad and S. Baroni: Turbo charging time-dependent density-functional theory
873 with Lanczos chains, Journal of Chemical Physics, 128(15), 14, doi: 10.1063/1.2899649, 2008.

874
875 Sanchez, M. A., T. Kling, T. Ishiyama, M. J. van Zadel, P. J. Bisson, M. Mezger, M. N. Jochum, J. D. Cyran,
876 W. J. Smit, H. J. Bakker, M. J. Shultz, A. Morita, D. Donadio, Y. Nagata, M. Bonn and E. H. G. Backus:
877 Experimental and theoretical evidence for bilayer-by-bilayer surface melting of crystalline ice,
878 Proceedings of the National Academy of Sciences of the United States of America, 114(2), 227-232, doi:
879 10.1073/pnas.1612893114, 2017.

880
881 Thompson, A. P., L. P. Swiler, C. R. Trott, S. M. Foiles and G. J. Tucker: Spectral neighbor analysis method
882 for automated generation of quantum-accurate interatomic potentials, Journal of Computational
883 Physics, 285, 316-330, doi: 10.1016/j.jcp.2014.12.018, 2015.

884
885 Tibshirani, R.: Regression shrinkage and selection via the lasso: a retrospective, Journal of the Royal
886 Statistical Society Series B-Statistical Methodology, 73, 273-282, doi: 10.1111/j.1467-9868.2011.00771.x,
887 2011.

888
889 Timrov, I., O. Andreussi, A. Biancardi, N. Marzari and S. Baroni: Self-consistent continuum solvation for
890 optical absorption of complex molecular systems in solution, Journal of Chemical Physics, 142(3), 9, doi:
891 10.1063/1.4905604, 2015.

892
893 Timrov, I., M. Micciarelli, M. Rosa, A. Calzolari and S. Baroni: Multimodel Approach to the Optical
894 Properties of Molecular Dyes in Solution, Journal of Chemical Theory and Computation, 12(9), 4423-
895 4429, doi: 10.1021/acs.jctc.6b00417, 2016.

https://doi.org/10.5194/acp-2021-875
Preprint. Discussion started: 1 November 2021

Atmospheric Chemistry and Physics Discussions

VandeVondele, J., M. Krack, F. Mohamed, M. Parrinello, T. Chassaing and J. Hutter: QUICKSTEP: Fast and accurate density functional calculations using a mixed Gaussian and plane waves approach, Computer Physics Communications, 167(2), 103-128, doi: 10.1016/j.cpc.2004.12.014, 2005.

Zhu, C. Z., B. Xiang, L. T. Chu and L. Zhu: 308 nm Photolysis of Nitric Acid in the Gas Phase, on Aluminum Surfaces, and on Ice Films, Journal of Physical Chemistry A, 114(7), 2561-2568, doi: 10.1021/jp909867a, 2010.